Beam fanning reversal in the ferroelectic relaxor $Sr_{0.61}Ba_{0.39}Nb_2O_6$ at high external electric fields

M. Goulkov
Institute of Physics, Science Ave 46, 03650, Kiev 39, Ukraine

M. Imlau
Department of Physics, University Osnabrück, Barbarastrasse 7, D-49069 Osnabrück, Germany

T. Granzow[a] and Th. Woike
Institute for Mineralogy and Geochemistry, University of Cologne, Zülpicherstrasse 49b, D-50674 Cologne, Germany

Beam fanning has been studied in the cerium-doped ferroelectric relaxor strontium–barium–niobate ($Sr_{0.61}Ba_{0.39}Nb_2O_6$:Ce, SBN:Ce) under the application of high external electric fields. Spatial reversal in the distribution of the scattered light is achieved both below and above the phase transition. It is shown that the photorefractive response in SBN strongly depends on the state of the polar structure of the crystal, which can be controlled by external fields. Coherent illumination of the crystal greatly facilitates the repoling process, causes a considerable refinement of the domain order in the ferroelectric phase and assists the stabilization of the polar structure in the relaxor regime. The model of scattering centers associated with refractive index anomalies located on domain walls is applied to receive detailed information about the distribution of initial seed scattering in the crystal bulk and the efficiency of nonlinear amplification of the scattering. © *2003 American Institute of Physics.* [DOI: 10.1063/1.1610234]

I. INTRODUCTION

Cerium-doped strontium–barium–niobate ($Sr_{0.61}Ba_{0.39}Nb_2O_6$:Ce, SBN:Ce) has received much attention in nonlinear optics since it exhibits a very strong photorefractive effect.[1,2] The incorporation of cerium extends the spectral range of the photorefractive response from the low ultraviolet up to the near-infrared and considerably increases the efficiency of the recording of refractive index gratings.[3,4] A spatially modulated light field induced by the interference of two coherent waves gives rise to a space-charge field E_{sc} due to a spatial redistribution of photoexcited charge carriers in the crystal volume. This periodic electric field modulates the refractive index of the crystal via the linear electro-optic effect so that a phase grating appears. In SBN with typical nonlocal photorefractive response, the refractive index grating is shifted with respect to the incoming light interference pattern. Mutual diffraction of the two recording waves on the shifted grating leads to the enhancement of one wave and the depletion of the other.[5] Thus, the nonlocal response gives rise to a stationary energy transfer between the two recording beams, called beam coupling, which is primarily responsible for many nonlinear optic effects including light-induced scattering.[6,7] The most efficient light-induced scattering in SBN is polarization-isotropic wide-angle scattering, which appears from a single laser beam[6] and is usually called beam fanning.[7] The incident beam is scattered at optical imperfections of the crystal. This initial scattering seeds the beam fanning. The seed waves record noisy photorefractive grat-

ings, so that beam coupling with the pump beam takes place. Scattered light of high intensity develops beside the directly transmitted pump beam in the directions where the seed scattering is effectively amplified. Therefore, it exhibits a very strong asymmetry in SBN in the plane of the polar c axis. Here, the direction and the efficiency of the energy transfer depend on the electro-optic coefficient r_{eff}. The sign and the absolute value of r_{eff} are determined by the vector of the spontaneous electric polarization $\mathbf{P}_s$.[8,9] Hence, photorefractive properties strongly depend on $\mathbf{P}_s$ and, respectively, on the domain structure of SBN. Control of the spontaneous polarization by an external electric field E_o allows deliberate manipulation of the photorefractive response. This becomes especially important for an application of photorefractive ferroelectrics in general as optical memories[10] and for optical data processing,[11] respectively.

In the last decade, certain attempts to manipulate the photorefractive properties of SBN via a spatial arrangement of the polar structure by external fields were made. The photorefractive optical hysteresis in SBN has already been demonstrated by two-beam coupling[12,13] and beam fanning[14] experiments, and was attributed to the ferroelectric hysteresis P_s-E_o. Also, the reversal of selected domain areas and the formation of ferroelectric domain gratings by exposure to light have been reported in SBN.[15,16] It was shown that the periodically modulated space-charge field induced by a sinusoidal light interference pattern assists the local reversal of the electric polarization in the fringes where the sum of the external field E_o and the space-charge field E_{sc} exceeds the coercive field E_c, $E_o+E_{sc}>E_c$. Furthermore, the specific effect of a locking of the polar structure by screening fields

---

[a]Electronic mail: tgranzow@uni-koeln.de

induced on the beam border was reported in incompletely illuminated SBN at slowly varying external fields in a beam fanning hysteresis experiment.[17]

Besides such very specific effects, where the light-induced space-charge field $E_{sc} \approx E_c$ assists the spatial arrangement of ferroelectric domains, coherent illumination has another very important impact on the polar structure that becomes apparent during the repoling of ferroelectrics using high electric fields $E_o \gg E_c$. Photoexcited charge carriers should actively participate in the compensation of local electric fields, which play an influential role in the appearance of ferroelectric domains in the crystal volume. Such charges should significantly affect the formation of the polar structure and the spatial arrangement of ferroelectric domains. This influence should especially be apparent in the vicinity of the phase transition and above. SBN is a relaxor ferroelectric. Therefore the polar structure does not decay at one well defined temperature, but in a quite large temperature interval. For SBN:Ce (0.66 mol %), ferroelectric domains are stable below the phase transition temperature $T_c = 55\,°C$.[18] Note that SBN has been shown to undergo a real phase transition,[19,20] so the term "phase transition temperature" is applicable for this relaxor system. The existence of polar clusters at $T > T_c$ causes a photorefractive effect and, respectively, beam coupling and light-induced scattering above the phase transition.[21] The relaxor behavior and the peculiarities of the polar structure in SBN at high temperatures are satisfactorily explained by the "random-field Ising model" (RFIM).[22,23] The central idea is that short-ranged randomly distributed electric fields cause interactions between neighboring elementary polar dipoles, which results in the formation of local regions with nonzero electric polarization (dipole clusters). These clusters constitute a polar structure in SBN at $T > T_c$, in a temperature range that will be referred to as "relaxor regime" in the following. At temperatures $T < T_c$, clusters turn into domains yielding very rich polar structures in the ferroelectric phase: both surface and bulk domains have been observed in SBN.[24] Poling of SBN by externally applied electric fields causes an alignment of most of the domains along the c axis, but does not significantly reduce their number. The presence of bulk domains is an important factor affecting the appearance of the initial scattering in SBN. According to the model of seed scattering proposed in Ref. 14, initial scattering originates from diffraction of the pump beam at optical inhomogeneities induced by electric fields localized at the domain tips. It is apparent that photoexcited charge carriers should affect magnitude and distribution of these scattering centers.

In this article we concentrate our attention on the study of the photorefractive response in highly doped SBN:Ce under externally applied electric fields much larger than inherent and light-induced fields in the crystal volume. The beam fanning has been chosen as the method for our investigations since it is the most basic photorefractive phenomenon. The experiments were carried out at different temperatures both below and above T_c.

Our investigations show that the beam fanning reversal is directly connected to the spatial reversal of the electric polarization in SBN. Its behavior strongly depends on the
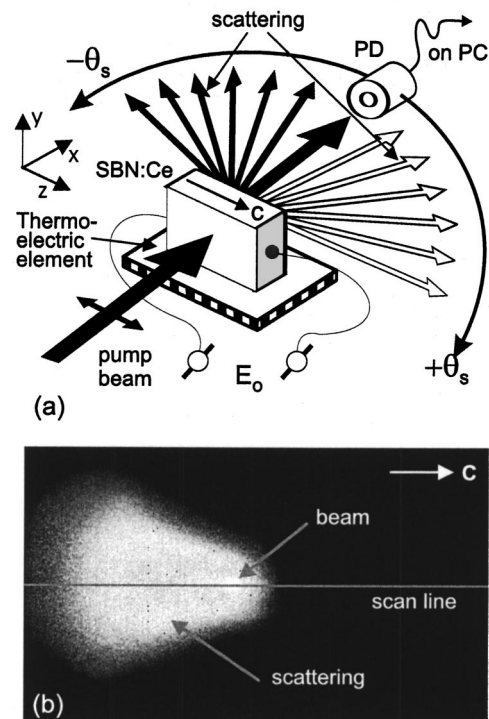
FIG. 1. (a) Experimental setup for measuring the angular distribution of scattered light in SBN:Ce. PD is a photodiode mounted on the rotating stage. The crystal is placed on a stack of Peltier elements to regulate the temperature; (b) Image of the scattering pattern on the screen behind the crystal at $T = 28\,°C$.

actual state of the polar structure. We found that coherent illumination of SBN significantly facilitates repoling and greatly promotes the stabilization of the polar structure in the crystal. Repoling performed on an illuminated sample ensures an instantaneous and complete reversal of the polar structure after only one iteration. Moreover, the scattering appears to be considerably enhanced after such repoling. Thus, the simultaneous application of electric field and illumination considerably refines the polar structure. Electric repoling of an unilluminated sample is less efficient and requires several repetitions to complete the reversal process, i.e., until a complete spatial reversal of the beam fanning is reached. The model of seed scattering in SBN is discussed in detail and applied to the experimental results.

II. EXPERIMENTAL SETUP

A single crystal of $Sr_{0.61}Ba_{0.39}Nb_2O_6$ doped with 0.66 mol % cerium was grown by the Czochralski technique and cut parallel to the crystallographic axes into a plate with dimensions of $5.65 \times 0.7 \times 2.75$ mm^3 along the crystallographic a-, b-, and c-axis, respectively. The sample was electrically poled by heating up to $140\,°C$, applying $E_o = 3.5$ kV/cm along the c axis and then slowly cooling back to room temperature before removing the field. After the poling process, the crystal was placed in the experimental setup, so that the polar c axis is initially oriented from the left- to the right-hand side of the sample as shown in Fig. 1(a). Note that the direction of the Cartesian **z** vector is always oriented

from the left to the right side. The temperature could be adjusted in the range of 10–150 °C with an absolute accuracy of 0.3 °C.

The unexpanded beam of a He–Ne laser ($\lambda = 633$ nm) with $1/e$-diameter $d = 0.8$ mm served as the pump beam and was directed normal to the large (a)–(c) face of the sample. Extraordinary light polarization was chosen. The beam intensity was set to $I_p = 70$ mW/cm^2 to prevent nonlinear effects other than light-induced scattering that might influence our measurements. The absorption coefficient of the sample was measured to 4 cm^{-1}.

The light-induced scattering pattern is usually observed on a screen (not shown in Fig. 1) placed behind the sample. To measure the angular intensity distribution $I_s(\theta_s)$ of the scattering pattern, a photodetector PD was mounted onto a motorized rotation stage at a distance of $L = 5.5$ cm behind the sample, allowing to measure $I_s(\theta_s)$ along the polar c axis in the angular range of $-90° \leq \theta_s \leq +90°$ (measured in air). Positive and negative scattering angles θ_s correspond to scattered light having positive and negative projections of the propagation vector on the z axis, respectively. At $\theta_s = 0°$, the photodetector crosses the pump beam directly behind the crystal, resulting in an intensity peak. The photodetector aperture limits the apex angle of the measured light to 0.5°. The entire setup was enclosed in a black box (not shown in Fig. 1) with only a small opening for the entrance of the pump beam to minimize the noise from external light sources.

To apply an external electric field E_o to the sample, the surfaces normal to the polar axis were covered with conducting silver paste and connected to a dc power supply. Fields applied in the same direction as during the poling procedure are considered as positive, while fields applied in the opposite direction are considered as negative. From the photorefractive hysteresis experiment performed at room temperature,[14] the coercive field in the sample was measured to $E_c = -1.5$ kV/cm, while total reversal of the spontaneous polarization was observed at -3 kV/cm. Therefore, $E_o = \pm 3.5$ kV/cm was chosen to perform the repoling process in our experiments. When applied, the magnitude E_o is established in 40 s in steps of 0.175 kV/cm with a lag time of 2 s between the steps. This time is short enough to neglect the impact of screening fields, induced around the beam, on the dynamics of repoling processes. The screening fields may affect the scattering distribution at small angles only in the steady state, because of additional changes of the refractive index on the border of the illuminated area. Two different procedures to apply the electric field and coherent illumination to the crystal were used.

Procedure 1. Simultaneous action of external field and illumination: The crystal is continuously illuminated by the pump beam, while the external field is applied and raised to the amplitude E_o. The field remains applied during the measurement of the angular distribution of beam fanning.

Procedure 2. Separate action of external field and illumination: The external field E_o is applied to the unilluminated crystal for 10 s and then switched off. After a relaxation time of about 1–2 min, the crystal is illuminated by the pump beam.

In both cases, $I_s(\theta_s)$ is measured after the steady state is reached. Below, we refer to the application of an external field with coherent illumination of the crystal after or during the action of the field E_o (depending on the chosen procedure 1 or 2) as a single iteration of the corresponding repoling procedure. If it is necessary, more than one iteration can be performed to complete the crystal repoling.

III. EXPERIMENTAL RESULTS

When SBN is illuminated by the laser beam, a bright diffusive strip of scattered light forms behind the crystal, reaching a steady state after a duration of 15 min under the chosen experimental conditions. The polarization of the scattered light is equal to that of the incoming laser light. The main part of the scattered light appears in the negative direction of the c axis of the crystal, which coincides with the z axis (negative scattering angles θ_s), when no external electric field is applied. The application of $E_o = -3.5$ kV/cm along the z axis causes a spatial inversion of the beam fanning (refered to as "forward reversal" in the following). Most of the scattered light is now directed to the positive direction of the z axis (positive scattering angles θ_s). When E_o is changed back to positive values, the beam fanning switches back to its initial distribution "backward reversal". We found that the spatial reversal of beam fanning occurs differently if SBN is illuminated either during or after the application of external fields. Furthermore, it is remarkably different in the ferroelectric phase ($T < T_c$) and in the relaxor regime ($T > T_c$):

A. Ferroelectric phase ($T < T_c$)

1. Simultaneous action of E_o and coherent illumination

The experimental results of the beam fanning reversal measured at $T = 47$ °C using procedure 1 are shown in Fig. 2(a). The bold curve a is the intensity distribution measured before a field is applied. The peak at $\theta_s = 0°$ is the intensity of the transmitted pump beam. $I_s(\theta_s)$ shows a strong spatial asymmetry: the broad maximum is located at negative angles around $\theta_s \approx -20°$, while at positive angles I_s is extremely low. Curve b represents $I_s(\theta_s)$ measured at $E_o = -3.5$ kV/cm. The light distribution is spatially reversed, so that the maximum is now found at $\theta_s \approx +20°$. The total scattering intensity calculated over the whole beam fanning profile increases after the reversal process (however, due to the logarithmic scale in Fig. 2 the difference between curves a and b is not remarkable). Note that the angular interval corresponding to the intensity of the transmitted pump beam is excluded from the calculation of the total scattering intensity. Obviously, application of the external field using procedure 1 allows a prompt and effective reversal of the beam fanning. Figure 2(b) shows $I_s(\theta_s)$ when a positive external field is applied afterwards: curve b is taken from Fig. 2(a) for better comparison, curve (c) is the beam fanning profile measured at $E_o = +3.5$ kV/cm, and curve d (greyscaled) shows $I_s(\theta_s)$ measured at $E_o = 0$ kV/cm after curve (c). Scattering maxima on curves (c) and (d) are found at the same angular position as on curve (a), but twice higher in intensity. The
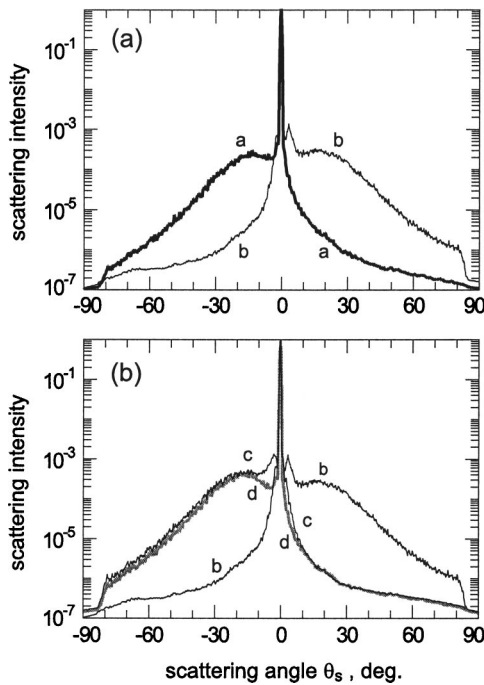
FIG. 2. Angular distribution of scattered light showing the beam fanning reversal in SBN in the ferroelectric state ($T=47\,°C$) performed according to procedure 1.(*a*) $E_o=0$ kV/cm; (*b*) forward reversal, $E_o=-3.5$ kV/cm; (*c*) backward reversal, $E_o=+3.5$ kV/cm; (*d*) $E_o=0$ kV/cm.

FIG. 3. Angular distribution of scattered light showing the beam fanning reversal in SBN in the ferroelectric state ($T=47\,°C$) performed according to procedure 2. (*a*) $E_o=0$ kV/cm; (*b*)–(*d*) first, second, sixth iterations of forward reversal, $E_o=-3.5$ kV/cm; (*e*)–(*g*) first, second, sixth iterations of backward reversal, $E_o=+3.5$ kV/cm.

total intensity measured in curve (*d*) is only marginally lower than in curve (*c*). Hence, the reversal of beam fanning to its initial state is as effective as the forward reversal. Further application of negative and positive external fields causes replicated forward and backward reversals; however, the absolute value of the maximum scattering intensity is no longer increased and remains the same as for curve (*c*). In addition to the broad maximum of the scattering distribution, there are additional small peaks at $\theta_s \approx \pm 3°$ in the data set of *b* and *c*, i.e., they appear only if a nonzero external field is applied.

2. Separate action of E_o and coherent illumination

The properties of the spatial reversal of the scattering distribution are changed if E_o is applied to the unilluminated sample (procedure 2). It turned out that complete spatial switching of beam fanning does not occur after the application of a negative electric field. Procedure 2 had to be repeated to reach a complete scattering reversal with respect to the amplitude of the initial scattering distribution. Several iterations of the forward and backward reversals are shown in Figs. 3(a) and 3(b), respectively. The bold curve *a* is the initial intensity distribution of the beam fanning. The first, second, and sixth iteration of the forward reversal process are given by the angular profiles (*b*), (*c*), and (*d*). Respectively, the profiles (*e*), (*f*), and (*g*) are the first, second, and sixth iterations of the backward reversal. A comparison of the profiles (*a*) and (b) shows that the direction of the beam fanning is reversed although the external field is applied to SBN without simultaneous coherent illumination. However, the total scattering intensity as well as the spatial asymmetry of the scattering distribution is considerably reduced. Both fea-

tures improve after repeated performing of procedure 2. After the sixth iteration, $I_s(\theta_s)$ finally becomes symmetric to profile (*a*). The same is true for the backward reversal, when the intensity distribution is gradually switched from profile (*d*) to profile (*g*) (greyscaled) in Fig. 3(b). Again, a complete reconstruction of the beam fanning is reached only after all six iterations: profile (*g*) in Fig. 3(b) is identical to curve (*a*) in Fig. 3(a). One should note that the increase of the scattered intensity after repeated application of E_o was observed only if every application of E_o is followed by an illumination of the crystal. Applying E_o six times without intermediate illumination of the crystal has the same effect as a single application, resulting in curve (*b*) [or (*e*)].
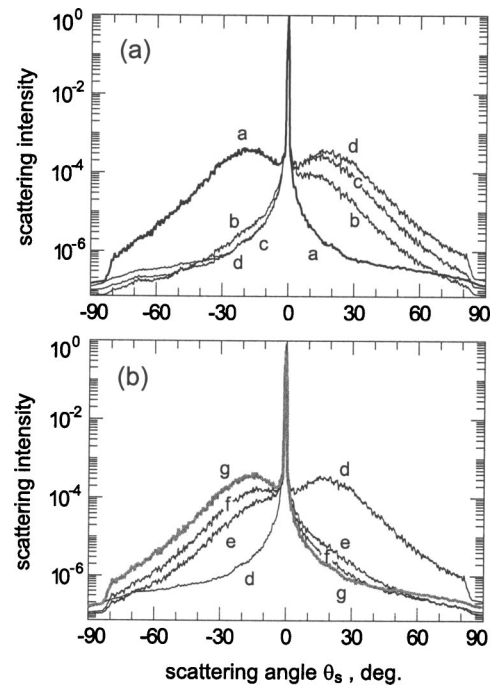
In summary, a fast and effective spatial reversal of the photorefractive response in SBN is possible by the application of high electric fields $E_o \gg E_c$ together with coherent illumination. An application of external fields without light exposure allows a gentle operation with the efficiency of the reversal processes.

B. Relaxor regime ($T>T_c$)

The response of the beam fanning on the repoling procedures 1 and 2 has also been studied in the relaxor regime at $T=57\,°C$. Here, $T>T_c$, but the crystal still possesses a nonzero macroscopic polarization P (Ref. 25) and shows a strong photorefractive effect.

1. Simultaneous action of E_o and coherent illumination

At $T>T_c$, the scattering is sensitive to the sign of E_o and exhibits both forward and backward reversal if E_o is

J. Appl. Phys., Vol. 94, No. 8, 15 October 2003

Goulkov *et al.* 4767
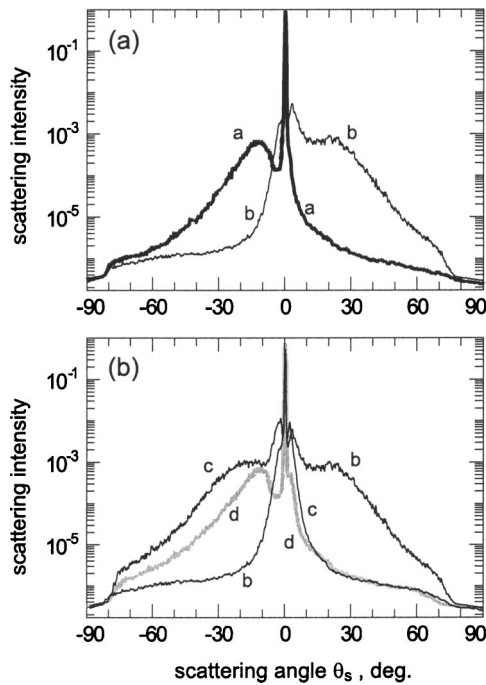
FIG. 4. Angular distributions of the scattered light showing the beam fanning reversals in SBN in the relaxor regime ($T = 57\,°C$) performed according to procedure 1. (*a*) $E_o = 0$ kV/cm; (*b*) forward reversal, $E_o = -3.5$ kV/cm; (*c*) backward reversal, $E_o = +3.5$ kV/cm; (*d*) $E_o = 0$ kV/cm.

FIG. 5. Angular distribution of scattered light showing the beam fanning reversal in SBN in the relaxor regime ($T = 57\,°C$) performed according to procedure 2. (*a*) $E_o = 0$ kV/cm; (*b*)–(*d*) first, second, sixth iterations of forward reversal, $E_o = -3.5$ kV/cm; (*e*)–(*g*) first, second, sixth iterations of backward reversal $E_o = +3.5$ kV/cm.

applied to the illuminated crystal. The sequence of the experimental curves in Fig. 4 is the same as in Fig. 2. An analysis of the data shows that the scattering reversal with procedure 1 in SBN in the relaxor regime is as effective as at $T < T_c$: a complete reversal is achieved with only one iteration. Figure 4(a) shows the forward reversal caused by a negative electric field: the bold curve (*a*) is the angular profile before the reversal, and curve (*b*) is the intensity distribution at $E_o = -3.5$ kV/cm. The backward reversal is shown in Fig. 4(b): curve (*b*) is taken from Fig. 4(a), curve (*c*) is measured at $E_o = +3.5$ kV/cm, curve (*d*) (greyscaled) is measured at $E_o = 0$ kV/cm after curve (*c*). A comparison of the profiles (*a*) in Figs. 2 and 4 shows that at zero field the increased temperature causes a decrease of the total scattering intensity, as well as an accumulation of scattered light at smaller angles θ_s.[17] $E_o \neq 0$ results in an effective angular widening of beam fanning profiles see, e.g., curves (*a*) and (*b*) in Fig. 4(a), and curves (*c*) and (*d*) in Fig. 4(b). The scattering shrinks back when the field E_o is switched off [(*d*) in Fig. 4(b)].

2. Separate action of E_o and coherent illumination

Figure 5(a) shows the forward beam fanning reversal when the external field is switched off before the sample is illuminated (procedure 2): The bold curve (*a*) is the initial angular profile, the curves (*b*), (*c*), and (*d*) show $I_s(\theta_s)$ after the first, second, and sixth application of $E_o = -3.5$ kV/cm. Figure 5(b) illustrates the backward reversal: curve (*d*) is $I_s(\theta_s)$ taken from the previous set, angular profiles (*e*), (*f*), and (*g*) (greyscaled) are measured after the first, second, and sixth applications of $E_o = +3.5$ kV/cm, respectively. It is evident from Fig. 5 that a complete scattering reversal is no longer achieved. Even after the sixth iteration, the total scattering intensity amounts only to 20% of the intensity measured in curve (*a*).

IV. DISCUSSION

To explain the observed differences in the behavior of the beam fanning reversal, we must take into account: (1) the dependence of the photorefractive properties of SBN:Ce on its polar structure; (2) the evolution of the polar structure if T approaches T_c; (3) the source for initial scattering that seeds the beam fanning, and the dependence of the seed scattering on external factors such as electric fields and coherent illumination. The following discussion takes these considerations into account.

Beam fanning is a kind of light-induced scattering and therefore a typical photorefractive phenomenon. It is initially seeded by diffraction or refraction processes of the incident beam at optical inhomogeneities in the crystal volume. Below, we follow the model of scattering centers in SBN as local anomalies of the index of refraction δn located at domain walls:[14] Nano- and microscale electric fields, inherent to SBN[26,27] and actually responsible for the existence of a rich variety of bulk ferroelectric domains in the crystal,[24,28] give rise to the refractive index changes δn via the linear electro-optic effect. These changes appear to be most efficient at domain tips. The size Λ of ferroelectric domains in SBN varies in the range of dozens of nanometers to dozens of micrometers.[29,30] Thus, the polar structure can be considered as a large number of sequences of domains distributed more or less regularly in the direction of the c axis. According to our model of seed scattering, δn anomalies located at tips of domains of the same size form a periodic sequence of
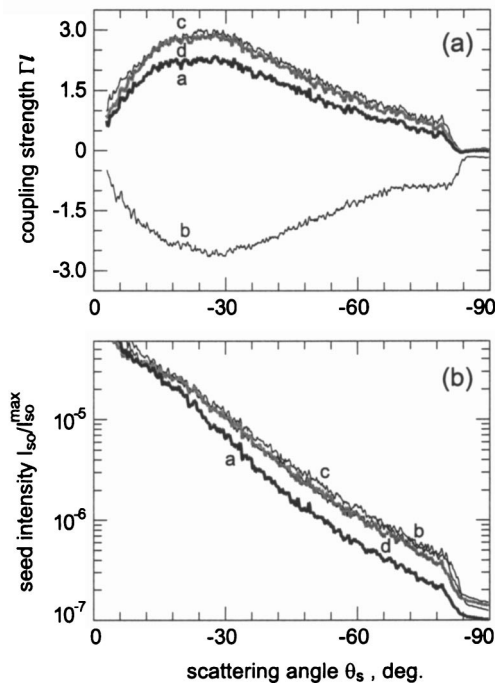
FIG. 6. Angular distribution of the coupling strength (*a*) and the seed scattering intensity (*b*) extracted from the beam fanning profiles in Fig. 2.

FIG. 7. Angular distribution of the coupling strength (*a*) and the seed scattering intensity (*b*) extracted from the beam fanning profiles in Fig. 3.

scattering centers with the corresponding spatial period Λ and result in the diffraction of the intensity I_{so} from the pump beam at the angle $\theta_s = 2 \arcsin [\lambda/(2\Lambda)]$. Diffraction at δn-structures with large Λ is characterized by smaller scattering angles θ_s, whereas structures with small Λ will result in large angles θ_s. It is also expected that perfectly aligned domain sequences result in well-ordered refractive index structures and in stronger seed scattering I_{so}, whereas the scattering originating from irregular δn structures located on disordered domains will be less effective. In our recent investigations of the beam fanning hysteresis in SBN:Ce (Ref. 14) we found that seed scattering in incompletely poled samples and in samples with a large amount of 180° domains is much weaker than in perfectly poled SBN with ferroelectric domains aligned in one direction. The deep minimum exhibited by the seed scattering at $E_o = E_c$, i.e., when the domain order is totally broken down and $P=0$, is proof for our model assumption. It should be noted, however, that the total intensity of the scattered light also depends on the size of the electro-optic coefficients: The sharp drop in transmitted intensity observed at temperatures near the phase transition[17] is due to this increase of r_{eff}, which counters the effects of a decrease of the seed scattering due to thermal domain disorder.

The process of writing holographic gratings with the incident beam (pump wave *p*) and the seed scattering (seed waves *s*) and the amplification of the scattered light is described in great detail in Refs. 14, 17, and 21. According to the spatial alignment of scattering centers in SBN along the polar axis, it is sensible to assume a symmetric distribution of the seed scattering I_{so} in $\pm c$ direction: $I_{so}(-\theta_s) = I_{so}(+\theta_s)$. Seed waves propagating at scattering angles $-\theta_s < 0$ ($-c$ direction) are exponentially amplified due to beam
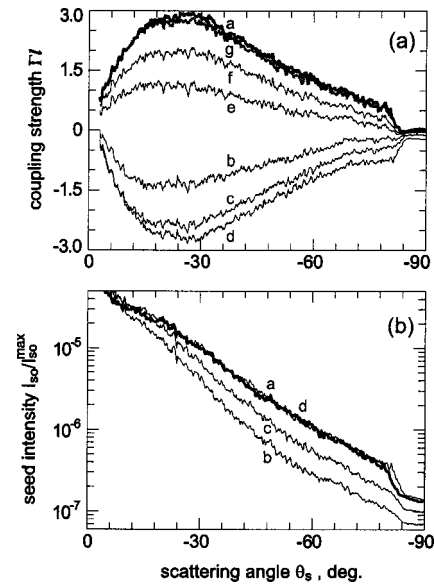
coupling with the pump wave *p*, whereas depletion takes place for $+\theta_s > 0$ ($+c$ direction). On the exit surface of the sample, I_s is given by $I_s^{\mp \theta_s} = I_{so} \exp(\pm \Gamma l)$. The product Γl is usually called coupling strength, where Γ is the coupling coefficient and l is the effective interaction length of seed and pump wave. A square-root product of $I_s^{-\theta_s}$ and $I_s^{+\theta_s}$ gives the intensity I_{so} equal for the two symmetric seed waves, while their logarithmic ratio gives the corresponding coupling strength:

$$I_{so}(\theta_s) = \sqrt{I_s^{-\theta_s} I_s^{+\theta_s}}, \qquad (1)$$

$$|\Gamma(\theta_s)| l = \frac{1}{2} \ln \left(\frac{I_s^{-\theta_s}}{I_s^{+\theta_s}} \right). \qquad (2)$$

Figures 6(a)–9(a) and 6(b)–9(b) show the angular dependence of Γl and I_{so} for $\theta_s < 0$, respectively, obtained from the $I_s(\theta)$ profiles shown in Figs. 2–5. For easier identification, the Γl and I_{so} curves are labeled identically to the corresponding original I_s profiles.

Before we start the particular analysis of changes in $\Gamma(\theta_s)$ and $I_{so}(\theta_s)$ resulting from the repoling procedures 1 and 2, we should consider some general relations between the polar structure and the beam fanning. The coupling coefficient is proportional to the electro-optic coefficient: $\Gamma \propto r_{33}$, which in turn depends on the macroscopic polarization P:[9]

$$r_{33} = 2 g_{33} P_s \varepsilon_{33} \varepsilon_o, \qquad (3)$$

where g_{33} is the quadratic electro-optic coefficient. $P_s > 0$ when the projection of the vector $\mathbf{P_s}$ on the *z* axis is positive, and $P_s < 0$ otherwise. Thus, the absolute value of P_s describes the efficiency of amplification of seed scattering, while its sign defines the direction of amplification and thereby the spatial orientation of the beam fanning. When the direction of P_s is inverted by applying an external electric field $E_o \gg E_c$, Γ changes its sign, resulting in the spatial
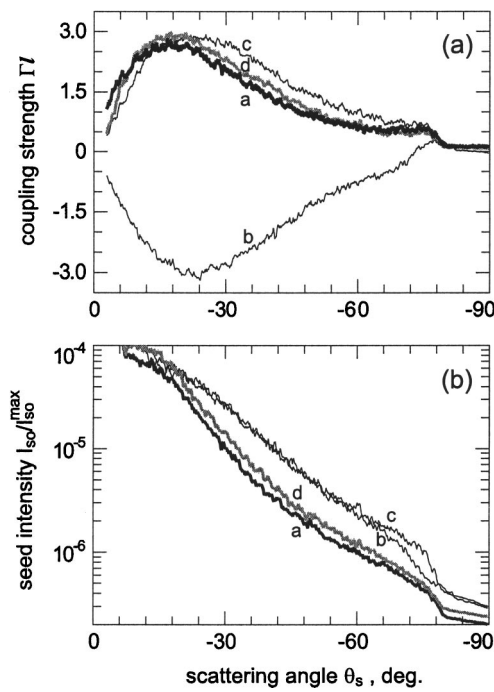
FIG. 8. Angular distribution of the coupling strength (*a*) and the seed scattering intensity (*b*) extracted from the beam fanning profiles in Fig. 4.

inversion of $I_s(\theta_s)$. An imperfect domain inversion and formation of 180° domains, which occurs in SBN during the repoling procedure, decreases the absolute values of P_s and r_{33}, respectively. As a result, Γ is reduced and the beam fanning is weakened. A decrease of r_{33} also results in a reduction of δn anomalies induced by internal electric fields located at domain tips. Moreover, the partial depolarization
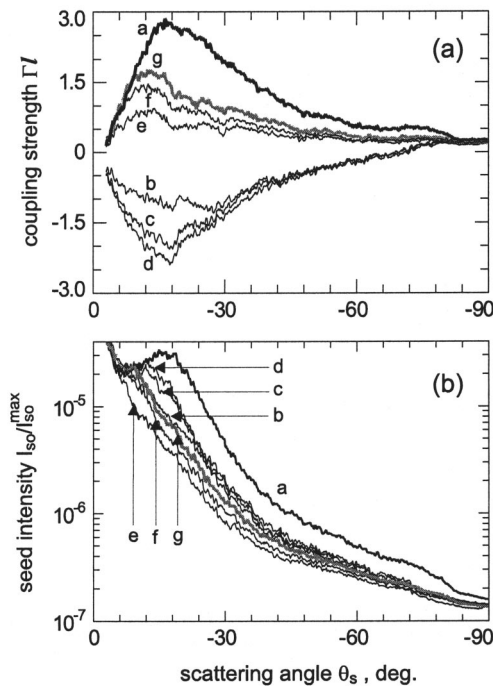
FIG. 9. Angular distribution of the coupling strength (*a*) and the seed scattering intensity (*b*) extracted from the beam fanning profiles in Fig. 5.

of SBN results in a disturbance of the regular sequences of scattering centers. These two reasons should cause a decrease of the seed scattering, as well as it may change its angular distribution. Hence, variations in the polar structure affect both I_{so} and Γ, and finally changes the beam fanning. At the same time, we have to remember that free electrons excited by coherent illumination play an important role in ferroelectrics[31] and particularly in repoling processes by modifying local electric fields in the crystal bulk.

A. Ferroelectric phase ($T < T_c$)

At $T = 47\,°C$, SBN is in the ferroelectric phase. The polar structure of the poled sample consists of domains aligned in one direction. Strong cooperative interaction guarantees stable alignment of domains. A single application of an external field $E_o > E_c$ to the illuminated SBN results in an immediate spatial forward and backward inversion of the beam fanning, depending on the sign of the electric field [see curves (*a*) and (*b*) in Fig. 2(a) and curves (*b*) and (*c*) in Fig. 2(b)]. At the same time, an application of the field to the unilluminated crystal results only in a partial reversal [see curves (*a*) and (*b*) in Fig. 3(a) and curves (*d*) and (*e*) in Fig. 3(b)]. These peculiarities can be explained by different changes of the spontaneous polarization achieved in SBN during repoling processes 1 and 2.

Using procedure 1, the crystal is illuminated by coherent light during the action of the external field. First, if $E_o < 0$ is applied, a part of the ferroelectric domains in the crystal volume flip following the direction of the field, but some domains, locked on local electric defects, will retain their initial orientation. If the crystal is illuminated, electrons are photoexcited from negatively charged centers, migrate in the crystal due to thermal diffusion as well as drift under the field E_o and are trapped on positively charged centers, leading to a compensation of local fields. Both processes of photoexcitation and trapping will lower potential barriers locking domains on defects, until the external field will flip the domains. The number of 180° domains should also be considerably reduced in this process. The refined polar structure causes a larger coupling coefficient Γ and a stronger seed scattering. Both results are illustrated by curves (*a*) and (*b*) in Figs. 6(a) and 6(b). The absolute values of Γl in curve (*b*) are higher than on the initial curve (*a*), but lower than in curve (*c*). This shows that an application of $E_o > 0$ results in a further refinement of the polar structure. Small differences between curves (*c*) and (*d*) mirror the increase of P induced by E_o: it vanishes after the field is switched off. The I_{so} curves show a similar behavior. The fact that all I_{so} curves in Fig. 6(b) converge at small scattering angles allows us to suggest, in particular, that large-scale domains are aligned with high regularity by the application of E_o.

One observes a different repoling behavior when using repoling procedure 2 instead of procedure 1. The partial inversion of the polar structure observed after the first iteration of process 2 can be explained as follows: When $E_o > 0$ is applied, most ferroelectric domains change their spatial orientation, but some domains remain locked by strong local fields and do not reverse their orientation. Posterior coherent illumination compensates the local fields by photoinduced

charge carriers, resulting in a lower potential barrier of the domains, but it does not invert their orientation. Therefore, a considerable reduction of scattered light is observed. E_o has to be applied again to switch further domains. The drastic difference in the results of beam fanning reversal obtained by the sixfold application of the external field with and without posterior illumination after the action of E_o unambiguously proves that, in our case, the coherent illumination is not only a method of observation, but also a means of assisting the repoling procedure.

The sharp submaxima observed in Fig. 2 at small θ_s possibly appear due to strong changes of the refractive index induced by screening fields on the border of the laser beam. These screening fields are formed owing to the drift of photoexcited electrons along the direction of the external field and the trapping of electrons on the border of the illuminated area. The separate action of E_o and illumination in procedure 2 provides no δn anomalies on the beam edge and no sharp submaxima near the transmitted beam in Fig. 3.

B. Relaxor regime ($T > T_c$)

At $T > T_c$, the cooperative interaction between the local dipoles is overcome by growing thermal energies, resulting in a breakdown of the domain structure into polar clusters stabilized by short-ranged random fields, causing a nonzero macroscopic polarization. The cluster structure slowly vanishes with increasing temperature, until a macroscopic polar structure can no longer be observed at $T > 90\,°C$. At $T = 57\,°C$, the temperature used in our experiment, our sample is already in the relaxor regime, where only dipole clusters exist.

The actual temperature of domain disordering depends on the dimension Λ of the domains: smaller domains disorder and vanish at lower temperatures. The disorder and decay of the polar structure of the dimension Λ should correlate with the rise of irregularities in scattering structures associated with the period Λ, and result in the strong reduction of seed scattering at the corresponding θ_s angles. Since small-scale structures (larger θ_s angles) disorder and decay earlier than large-scale structures (smaller θ_s angles), the scattering maximum will shift from larger to smaller angles with increasing temperature: compare curves (*a*) in Figs. 2(a) and 3(a) ($T = 47\,°C$) with curves (*a*) in Figs. 4(a) and 5(a) ($T = 57\,°C$), all measured at zero field. However, application of E_o reestablishes the polar structure and restores the initial $I_s(\theta_s)$ distribution. At $E_o = 0$, thermal disorder again sets in, and the maximum of $I_s(\theta_s)$ is again shifted to smaller scattering angles [see curves (*d*) and (*c*) in Fig. 4(b)]. In this temperature range of thermally unstable polar clusters, the process of beam fanning reversal may very well differ from that in the ferroelectric phase.

If the repoling is performed under illumination (procedure 1), E_o aligns dipole clusters along one preferential direction. The reestablishment of the polar order improves the regularity of the scattering centers, particularly for small-scale structures. This results in an increase of the averaged values of the macroscopic polarization P and Γ, and in a considerable enhancement of the seed scattering intensities at large angles θ_s. The last effect is apparent from a comparison of curve (*a*) ($E_o = 0\,kV/cm$) and (*b*) ($E_o = -3.5\,kV/cm$), or (*c*) ($E_o = +3.5\,kV/cm$) and (*d*) ($E_o = 0\,kV/cm$) in Fig. 8(b). The large slope of curves (*a*) and (*d*) starting at $\theta_s = 18°$ indicates that clusters with $\Lambda < 2\,\mu m$ are thermally disordered at $E_o = 0$, while the spatial alignment of clusters with larger dimensions is not affected. The changes in the angular behavior of Γl due to the externally applied electric field agree with the corresponding changes in I_{so}. Figure 8(a) shows that the polar reversal at $T > T_c$, does not differ too much from that at $T < T_c$. The complete inversion of the polar structure is confirmed by different signs and mutually symmetric shapes of profiles (*b*) ($E_o = -3.5\,kV/cm$) and (*c*) ($E_o = +3.5\,kV/cm$) of Γl in Fig. 8(a), and by the corresponding profiles (*b*) and (*c*) of I_{so} shown in Fig. 8(b).

The situation changes if the beam fanning reversal is performed without illumination (procedure 2). Here, the repoling entails a strong reduction of the total scattering intensity because of dramatic changes in the spatial order of dipole clusters. The new polar direction established by $E_o < 0$ remains stable only as long as the field is applied to the crystal. In addition to a chaotic impact of the thermal disorder, the clusters are strongly affected by uncompensated internal fields trying to reverse the polar structure into the state observed before the spatial reversal. The lack of free electrons allows no compensation of these fields, which would stabilize the clusters in the reversed positions. Most mobile domains settle back immediately after the field is switched off, with a larger likelihood for small domains to return to the initial state. This backswitching disturbs the order of the polar structure and breaks the regularity in the corresponding sequences of the scattering centers, resulting in a strong suppression of seed scattering [curve (*b*) in Fig. 9(b)], a reduction of P_s and Γ [curve (*b*) in Fig. 9(a)], and, consecutively, a weakened beam fanning [curve (*b*) in Fig. 5(a)]. Complete reversal of the polar structure is impossible using procedure 2: Even after the sixth application of $E_o < 0$, neither Γl nor I_{so} reaches the values achieved before the repoling process [curves (*a*) and (*d*) in Figs. 9(a) and 9(b)]. The posterior application of $E_o > 0$ does not improve the situation, but results in further disordering: The I_{so}-profile (*g*) in Fig. 9(b) is even lower than profile (*b*), and profile (*g*) of the coupling strength Γl in Fig. 9(a) amounts in the maximum only to half the corresponding value on the initial profile (*a*).

V. CONCLUSION

To reverse the orientation of the polar structure in SBN:Ce, procedure 1 is significantly more effective than procedure 2. Simultaneous action of high external fields with illumination ensures the complete repoling of SBN in only one iteration and essentially refines and stabilizes the polar structure both at $T > T_c$ and at $T < T_c$. Separate and consecutive action of E_o and illumination results in a gradual step-by-step domain reversal in the ferroelectric phase, while it causes a significant spatial disorder in the polar structure in the relaxor regime.

ACKNOWLEDGMENT

[1] V. V. Voronov, E. H. Gulanyan, I. R. Dorosh, Yu. S. Kuzminov, A. L. Mikaelyan, V. V. Osiko, N. M. Polozkov, and A. M. Prokhorov, Sov. J. Quantum Electron. **6**, 1993 (1979).

[2] M. D. Ewbank, R. R. Neurgaonkar, W. K. Cory, and J. Feinberg, J. Appl. Phys. **62**, 374 (1987).

[3] G. A. Rakuljic, K. Sayano, A. Agranat, and A. Yariv, Appl. Phys. Lett. **53**, 1465 (1988).

[4] E. J. Sharp, M. J. Miller, G. J. Salamo, W. W. Clark, and R. R. Neurgaonkar, Ferroelectrics **87**, 335 (1988).

[5] P. Yeh, *Introduction to Photorefractive Nonlinear Optics* (Wiley, New York, 1993).

[6] V. V. Voronov, I. R. Dorosh, Yu. S. Kuz'minov, and N. V. Tkachenko, Sov. J. Quantum Electron. **10**, 1346 (1980).

[7] J. Feinberg, J. Opt. Soc. Am. **72**, 46 (1982).

[8] A. M. Prokhorov and Yu. S. Kuz'minov, *Ferroelectric Crystals for Laser Radiation Control* (Adam Hilger, Bristol, 1990).

[9] A. J. Fox, J. Appl. Phys. **44**, 254 (1973).

[10] J. E. Ford, J. Ma, and Y. Fainman, J. Opt. Soc. Am. A **9**, 1183 (1992).

[11] P. Yeh and A. E. Chiou, Opt. Lett. **12**, 138 (1987).

[12] T. Woike, T. Volk, U. Dörfler, R. Pankrath, L. Ivleva, and M. Wöhlecke, Ferroelectr. Lett. Sect. **23**, 127 (1998).

[13] T. Volk, L. Ivleva, P. Lykov, D. Isakov, V. Osiko, and M. Wöhlecke, Appl. Phys. Lett. **79**, 854 (2001).

[14] M. Yu. Goulkov, T. Granzow, U. Dörfler, Th. Woike, M. Imlau, and R. Pankrath, Appl. Phys. B: Lasers Opt. **76**, 457 (2003).

[15] F. Kahmann, R. Pankrath, and R. A. Rupp, Opt. Commun. **107**, 6 (1994).

[16] A. S. Kewitsch, M. Segev, A. Yariv, G. J. Salamo, T. W. Towe, E. J. Sharp, and R. R. Neurgaonkar, Phys. Rev. Lett. **73**, 1174 (1994).

[17] M. Goulkov, M. Imlau, R. Pankrath, T. Granzow, U. Dörfler, and Th. Woike, J. Opt. Soc. Am. B **20**, 307 (2003).

[18] T. Granzow, Th. Woike, W. Rammensee, M. Wöhlecke, M. Imlau, and R. Pankrath, Phys. Status Solidi A **197**, R2 (2003).

[19] J. Dec, W. Kleemann, V. Bobnar, Z. Kutnjak, A. Levstik, R. Pirc, and R. Pankrath, Europhys. Lett. **55**, 781 (2001).

[20] R. Blinc, A. Gregorovic, B. Zalar, R. Pirc, J. Seliger, W. Kleemann, S. G. Lushnikov, and R. Pankrath, Phys. Rev. B **64**, 134109 (2001).

[21] M. Goulkov, M. Imlau, R. Pankrath, T. Granzow, U. Dörfler, Th. Woike, and W. Kleemann, Opt. Commun. **218**, 173 (2003).

[22] V. Westphal, W. Kleemann, and M. D. Glinchuk, Phys. Rev. Lett. **68**, 847 (1992).

[23] W. Kleemann, Int. J. Mod. Phys. B **7**, 2469 (1993).

[24] G. Fogarty, B. Steiner, M. Cronin-Golomb, U. Laor, M. H. Garrett, J. Martin, and R. Uhrin, J. Opt. Soc. Am. B **13**, 2636 (1996).

[25] T. Granzow, U. Dörfler, Th. Woike, M. Wöhlecke, R. Pankrath, M. Imlau, and W. Kleemann, Appl. Phys. Lett. **80**, 470 (2002).

[26] W. Kleemann, Phase Transitions **65**, 141 (1998).

[27] W. Kleemann, J. Korean Phys. Soc. **32**, S853 (1998).

[28] N. R. Ivanov, T. R. Volk, L. I. Ivleva, S. P. Chumakova, and A. V. Ginszerg, Crystallogr. Rep. **47**, 1023 (2002).

[29] P. Lehnen, W. Kleemann, Th. Woike, and R. Pankrath, Phys. Rev. B **64**, 224109 (2001).

[30] P. Lehnen, J. Dec, W. Kleemann, Th. Woike, and R. Pankrath, Ferroelectrics **268**, 113 (2002).

[31] V. M. Fridkin, *Photoferroelectrics* (Springer, New York, 1979).